Nanoscale

PAPER

View Article Online
View Journal | View Issue

Check for updates

Cite this: *Nanoscale*, 2022, **14**, 2771

Highly luminescent red-emitting In(Zn)P quantum dots using zinc oxo cluster: synthesis and application to light-emitting diodes†

Yonghoon Choi,‡[a] Dohoon Kim,‡[b] Yun Seop Shin,[a] Woojin Lee,[a] Seungjin Orr,[c] Jin Young Kim *[a] and Jongnam Park *[a,d]

Despite the importance of separating nucleation steps from growth steps for the production of monodisperse highly luminescent In(Zn)P quantum dots (QDs), the practical implementation of this strategy is hindered by the high reactivity and fast depletion of conventional P precursors. This problem can be mitigated through the use of (i) Zn oxo clusters, which effectively regulate the kinetics of QD growth and prevent the fast depletion of conventional P precursors in the nucleation step, or (ii) seed-mediated continuous growth methods, which avoid secondary nucleation in the growth step and yield red-emitting InP QDs. Herein, we combine approaches (i) and (ii) to synthesize red-emitting In(Zn)P QDs with a high photoluminescence quantum yield (>93%) and a low emission bandwidth (full width at half maximum = 38 nm), revealing that our strategy hinders the carboxylate ketonization-induced generation of byproducts and suppresses the surface oxidation of In(Zn)P QDs during growth steps. The prepared In(Zn)P QDs are used to fabricate QD light-emitting diodes with a maximum brightness of 1164 cd m^{-2} and an external quantum efficiency of 3.61%. Thus, our results pave the way to the replacement of toxic Cd- and Pb-based QDs with more eco-friendly Zn- and In-based analogs for a variety of applications.

Received 7th December 2021,
Accepted 24th January 2022

DOI: 10.1039/d1nr08038e

rsc.li/nanoscale

Published on 04 February 2022. Downloaded by Yunnan University on 8/23/2025 9:48:06 PM.

1. Introduction

Colloidal quantum dots (QDs) exhibit superior optical properties, *e.g.*, high photoluminescence quantum yields (PLQYs), narrow emission bandwidths, high absorption cross-sections, and tunable emission wavelengths, thus finding numerous applications in bio-imaging, solar cells, and light-emitting diodes.[1–12] State-of-the-art Cd- and Pb-based QDs have ideal optical properties with high PLQYs (~100%) and narrow full widths at half maximum (FWHMs, <30 nm).[13,14] However, policies restricting the use of hazardous substances discourage the usage of Cd and Pb and necessitate the development of less toxic QDs.[15]

As representative non-toxic III–V QDs with competitive optical properties, InP QDs are promising alternatives to their Cd- and Pb-based counterparts.[16,17] The synthesis of monodisperse QDs relies on the separation of nucleation steps from growth steps after the injection of highly reactive precursors.[18] However, the rapid consumption of such highly reactive precursors (*e.g.*, tris(trimethylsilyl)phosphine (TMS_3P) as a common P precursor)[19] hinders this separation, favors Ostwald ripening, and, hence, broadens the size distribution of InP QDs. Although Ostwald ripening can be avoided through the use of less reactive P precursors such as tris(trimethylgermyl)phosphine, tri(pyrazolyl)phosphane, aminophosphine, and white phosphorus,[20–25] the optical properties of the resulting InP QDs do not satisfy industrial criteria.

The growth kinetics of InP can be controlled through the use of suitable Zn precursors such as Zn carboxylates. In particular, Zn oxo cluster ($[Zn_4O(oleate)_6]$ and $[Zn_7O_2(oleate)_{10}]$) produced by the thermal decomposition of Zn carboxylates at high temperature can effectively react with TMS_3P to afford a Zn–phosphine complex and thus hinder the reaction between TMS_3P and the In precursor.[26] The formation of this complex allows one to regulate the kinetics of In(Zn)P growth and successfully produce In(Zn)P QDs with superior optical properties, *e.g.*, narrow FWHM (37 nm) and high PLQY (95%). Moreover, In(Zn)P cores synthesized using Zn oxo cluster as Zn precursors have higher Zn contents than those produced using Zn carboxylates. The incorporation of Zn atoms into the

[a]*School of Energy and Chemical Engineering, Ulsan National Institute of Science and Technology (UNIST), Ulsan 44919, Republic of Korea. E-mail: jnpark@unist.ac.kr*
[b]*DUKSAN Techopia Co., Ltd, Cheonan 31217, Republic of Korea*
[c]*STMicroelectronics, Inc., 2755 Great America Way, Santa Clara, CA 95054, USA*
[d]*Department of Biomedical Engineering, Ulsan National Institute of Science and Technology (UNIST), Ulsan 44919, Republic of Korea*

†Electronic supplementary information (ESI) available. See DOI: 10.1039/d1nr08038e

‡These authors contributed equally to this work.

Published on 04 February 2022. Downloaded by Yunnan University on 8/23/2025 9:48:06 PM.

InP lattice results in its contraction and structural stabilization,[27,28] thus decreasing the content of surface defects and the contribution of nonradiative recombination to yield highly luminescent In(Zn)P QDs.

Despite the growing interest in red-emitting InP QDs, they remain less explored than green-emitting InP QDs. In view of the limitations of emission wavelength control *via* shell thickness adjustment, the realization of large InP cores with a highly monodisperse size distribution is of key importance for the production of red-emitting In(Zn)P QDs with superior optical properties.[29] However, the synthesis of large InP cores is challenged by the high covalency of In–P bonding and the high reactivity of P precursors,[30] while the additional injection of highly reactive P precursors for the growth of InP cores may induce secondary nucleation and promote Ostwald ripening. This secondary nucleation can be prevented using seed-mediated continuous growth methods, which rely on the slow injection of In–P or (Zn)In–P complexes *via* a syringe pump[31–33] and afford red-emitting InP QDs with high PLQYs (>90%) and narrow FWHMs (35–42 nm).

Herein, we prepare monodisperse highly luminescent red-emitting In(Zn)P QDs by seed-mediated continuous growth using a Zn oxo cluster as a Zn precursor, optimize the reaction parameters, compare the effect of the Zn precursor (Zn oleate *vs.* Zn oxo cluster) on QD growth, and reveal the origin of high QD quality. The optimal reaction parameters are used to synthesize narrow-FWHM (~38 nm) high-PLQY (>93%) red-emitting In(Zn)P/ZnSeS QDs based on high-quality In(Zn)P cores (quantum yield >40%). Finally, to demonstrate the practical utility of the prepared In(Zn)P QDs, we use them to fabricate QD light-emitting diodes (QLEDs).

2. Results and discussion

2.1. Optical properties of red-emitting In(Zn)P QDs produced by Zn carboxylates precursor and Zn oxo cluster

In view of the limited number of available P precursors, red-emitting InP QDs are far less explored than their green-emitting counterparts. Moreover, the growth of InP QDs requires a supply of additional In and P precursors, as the TMS_3P injected at the nucleation stage is rapidly consumed. Some groups have successfully synthesized red-emitting InP QDs using seed-mediated continuous growth and successive ionic layer adsorption and reaction methods,[31–33] both of which are usually adopted to prepare large III–V (*e.g.*, InP and InAs) nanoparticles.[34] Herein, we used seed-mediated continuous growth to prepare red-emitting In(Zn)P QDs with a narrow size distribution. In(Zn)P seeds were synthesized by the injection of a TMS_3P solution into reaction mixture, and the (Zn)In–P complex was then slowly introduced until In(Zn)P cores of the desired size were obtained (Fig. 1).

To investigate the effects of the Zn precursor on the optical properties of In(Zn)P cores, we compared a conventional Zn carboxylate precursor (Zn oleate (ZnOL)) with the Zn oxo cluster (Fig. 2) under identical conditions. The Zn precursors

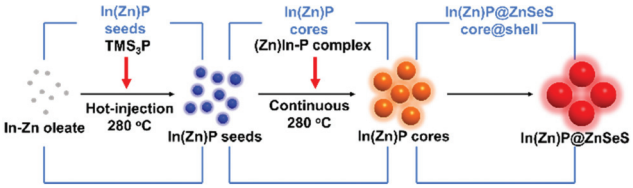

Fig. 1 Schematic synthesis of red-emitting In(Zn)P@ZnSeS QDs.

were introduced during the nucleation process of In(Zn)P seeds due to their reaction kinetics regulator property which influenced on the quality of QDs.[26] In(Zn)P seeds were synthesized by the hot injection of the TMS_3P solution, and the (Zn)In–P complex was then slowly introduced by a syringe pump. Each reaction batch was sampled after every 1 mL of the injected (Zn)In–P complex, and the specimens were subjected to UV-Vis and PLQY measurements without further purification.

In view of the regulatory effect of the Zn oxo cluster on reaction kinetics, the growth of In(Zn)P QDs occurred more slowly than in the case of ZnOL (Fig. S1†). As the duration of core growth increased from 1 to 5 h, the first exciton peaks of In(Zn)P cores produced using the Zn oxo cluster and ZnOL shifted from 446 to 526 nm and from 497 nm to 595 nm, respectively. Moreover, the first exciton peaks of Zn oxo cluster-derived QDs were sharper than those of ZnOL-derived QDs, which indicated a narrower size distribution of In(Zn)P cores in the former case (Fig. 2a and d). In addition, much narrower PL emissions were observed for Zn oxo cluster-derived QDs than for ZnOL-derived ones (FWHM = 38 and 66 nm, respectively) (Fig. 2b and e). The size distribution of In(Zn)P seeds was measured using dynamic light scattering (DLS) and was more narrow in the case of the Zn oxo cluster (Fig. S2†). Although the UV-vis spectrum of In(Zn)P seeds looks like the absorption of unreacted precursors (Fig. 2a), the TEM images of In(Zn)P seeds and 3 h-growth In(Zn)P cores showed the formation of In(Zn)P seeds and gradual growth by seed-mediated continuous growth (Fig. S3†). Thus, the observed trends were similar to those reported in our previous paper,[26] where we revealed that Zn oxo cluster can be used to generate Zn–phosphine complexes and regulate the kinetics of In(Zn)P core synthesis for obtaining In(Zn)P QDs with enhanced size uniformity. The conditions used to prepare the Zn oxo cluster also affected the quality of In(Zn)P QDs (Fig. 2). Because Zn oxo cluster can regulate reaction kinetics of In(Zn)P QDs,[26] the quality of Zn oxo cluster was important factor to produce high quality In(Zn)P QDs. For example, if the Zn oxo cluster was prepared using a short thermal decomposition time (~1 h), the In(Zn)P cores had a broader FWHM (~48 nm at an emission wavelength of 580 nm). Cores with optimal optical properties (FWHM ≈ 40 nm at an emission wavelength of 580 nm) were obtained using a decomposition time of 2.5 h. Higher than optimal decomposition times induced the formation of ZnO nanoparticles which lost their reaction kinetics regulating property and afforded In(Zn)P cores with a broad FWHM

 This journal is © The Royal Society of Chemistry 2022

Published on 04 February 2022. Downloaded by Yunnan University on 8/23/2025 9:48:06 PM.

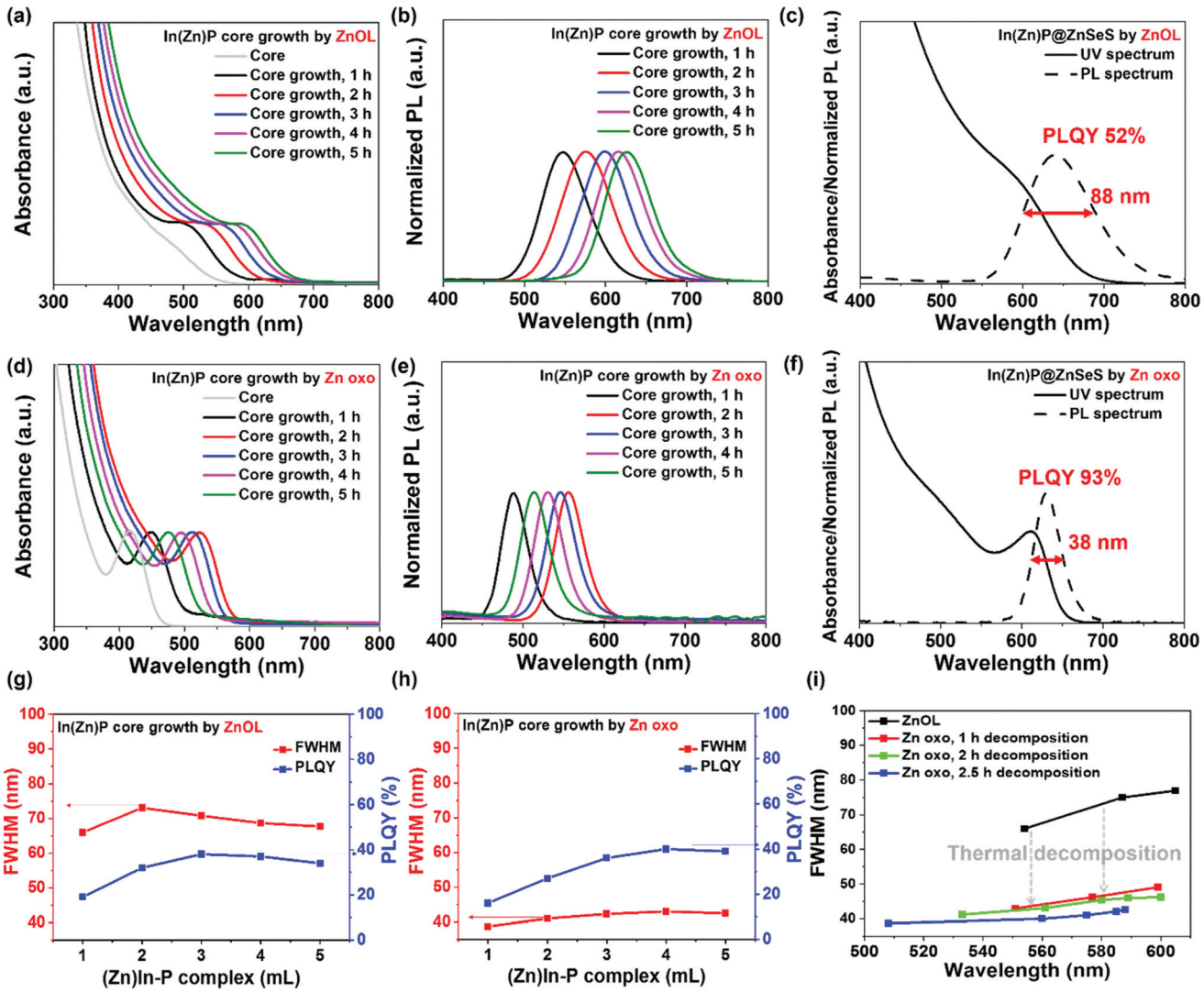

Fig. 2 (a and d) UV-vis and (b and e) PL spectra of In(Zn)P cores synthesized from (a and b) ZnOL and (d and e) the Zn oxo cluster using (Zn)In–P complex volumes of 0–5 mL. FWHMs and PLQYs of In(Zn)P@ZnSeS QDs with similar red emission prepared using (c) the ZnOL and (f) the Zn oxo cluster. Dependence of the FWHM and PLQY of In(Zn)P cores prepared from (g) ZnOL and (h) Zn oxo cluster as precursors on the volume of the added (Zn)In–P complex solution. (i) Effect of the duration of Zn oxo cluster decomposition on the FWHM of the prepared In(Zn)P cores, with data for cores prepared using ZnOL provided as a reference.

(46 nm) (Fig. S4†). InP cores are known to have poor luminescent properties (PLQY ≈ 1%). However, the large In(Zn)P cores synthesized herein had relatively high quantum yields of 30–40% despite the absence of inorganic semiconductor shells (Fig. 2g and h), which was attributed to the effective passivation of surface defects by either Zn precursor. This hypothesis was validated using time-resolved photoluminescence (TRPL) measurements, which revealed that the average decay lifetime (τ_{avg}) increased after seed-mediated continuous growth (Table S1†). The crystal structures of In(Zn)P cores and In(Zn)P@ZnSeS QDs were investigated by X-ray diffraction (XRD) measurement (Fig. S5†). XRD pattern of In(Zn)P cores was well-matched with zinc blende InP (JCPDS no. 32-0452) and that of In(Zn)P@ZnSeS QDs was observed between zinc blende ZnSe (JCPDS no. 37-1463) and zinc blende ZnS (JCPDS no. 05-0566) which indicated successful shell coating of ZnSeS layers. In addition to the crystal structures, we can observe the slight peak shift of (220) and (311) facet of In(Zn)P cores toward higher diffraction angle which means that our In(Zn)P cores have alloyed structures (Fig. S5†).

We conducted another control experiment using In laurate ($InLA_3$) rather than $InCl_3$ (Fig. S6†) in view of the poor initial optical properties of In(Zn)P seeds synthesized from $InCl_3$ and ZnOL (FWHM = 66 nm). By changing the In precursor from $InCl_3$ to $InLA_3$, we achieved a narrow initial FWHM of 38 nm, however, the FWHM of In(Zn)P cores increased (86 nm) after seed-mediated continuous growth. Moreover, the PL spectra of In(Zn)P cores synthesized using $InLA_3$ and ZnOL featured multiple emissions, which indicated the occurrence of secondary nucleation during growth. As the amount of carboxylates in

Published on 04 February 2022. Downloaded by Yunnan University on 8/23/2025 9:48:06 PM.

the growth system increased in the order of $InCl_3$ + Zn oxo cluster < $InCl_3$ + ZnOL < $InLA_3$ + ZnOL, we assumed that high carboxylate amounts adversely affected the optical properties of In(Zn)P cores during seed-mediated continuous growth. The effects of carboxylates in growth systems are discussed in detail below.

2.2. Effects of the Zn precursors on the surface defects and size distribution of red-emitting In(Zn)P QDs

The large FWHM was mainly ascribed to the surface defects and size polydispersity of QDs. To investigate the effect of the Zn precursor on the surface defects of In(Zn)P cores, we probed In(Zn)P QDs by TRPL measurements (Fig. S7†), fitted the data with a triexponential function, and extracted the relevant data (Table S1†). The fast decay components were related to intrinsic charge transfer processes in cores, while intermediate components were related to the intrinsic recombination of initially populated neutral states, and long-lived components were attributed to trap state emissions.[35] Notably, upon going from In(Zn)P seeds to In(Zn)P cores, the contribution of the long-lived component increased from 0.17 to 0.48 for ZnOL but decreased from 0.29 to 0.21 for the Zn oxo cluster which means that there were less surface trap state emission in In(Zn)P cores produced by Zn oxo cluster. Next, we measured temperature-dependent PL spectra to compare surface trap emission of In(Zn)P QDs (Fig. 3a and b). With decreasing temperature, the band-edge emission of In(Zn)P QDs were shifted to the short-wavelength and became sharper for both Zn precursors, as is commonly observed for low-temperature steady-state PL spectra because of lower thermal

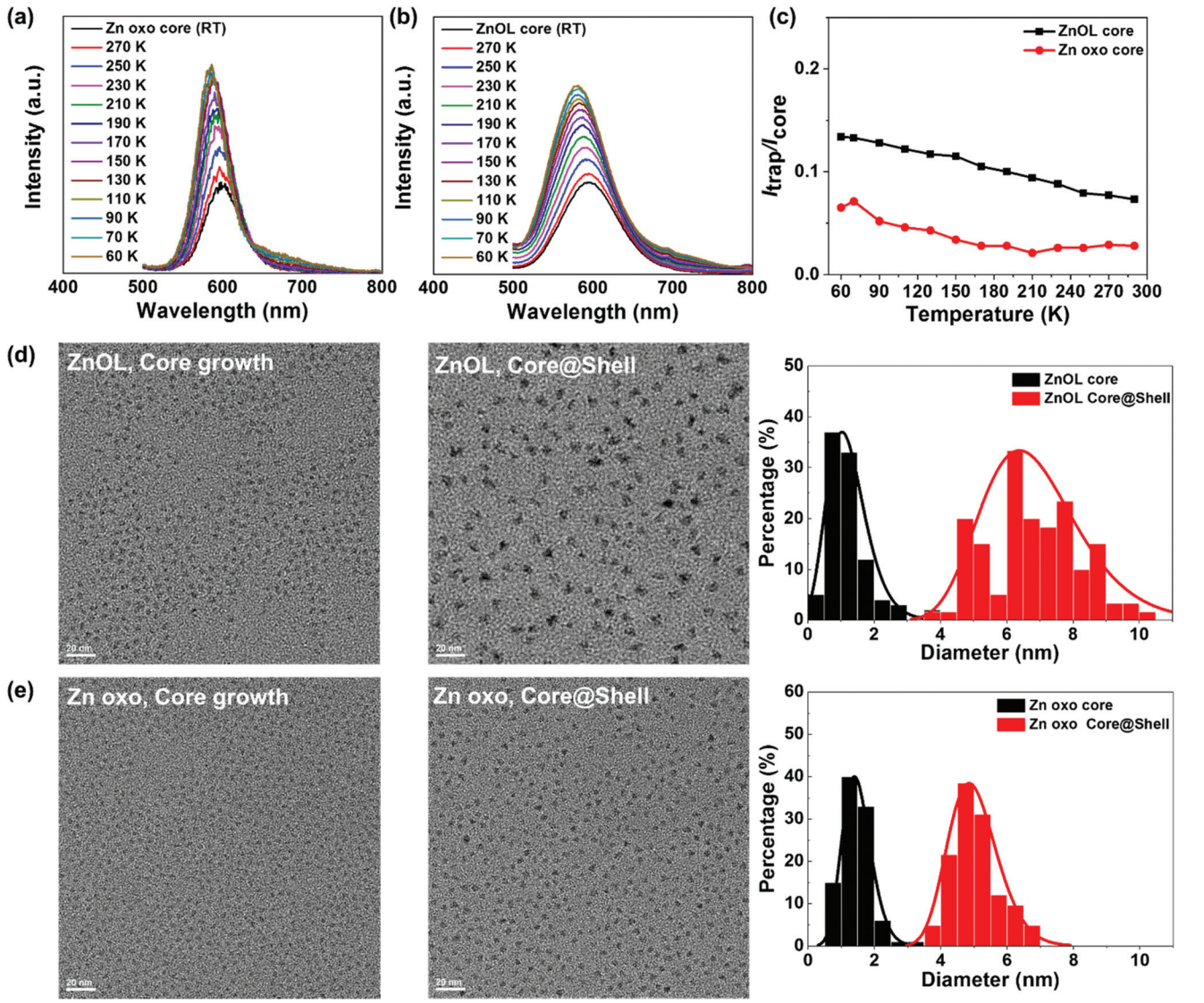

Fig. 3 Temperature-dependent PL spectra of In(Zn)P cores having 600 nm emission wavelength prepared using (a) the Zn oxo cluster and (b) the ZnOL. (c) Low-energy trap emission (~700 nm)/band edge emission intensity ratio (I_{trap}/I_{core}) as a function of temperature. TEM images and size distributions of In(Zn)P cores (emission = 600 nm) and In(Zn)P@ZnSeS QDs (emission = 620 nm) synthesized using (d) ZnOL and (e) the Zn oxo cluster.

 This journal is © The Royal Society of Chemistry 2022

Published on 04 February 2022. Downloaded by Yunnan University on 8/23/2025 9:48:06 PM.

energy. The ratio of low-energy trap emission (~700 nm) to band edge emission was plotted as a function of temperature (Fig. 3c) to reveal that the fraction of surface defect emission was lower for In(Zn)P cores prepared from Zn oxo cluster.

The size distribution of In(Zn)P QDs was probed by TEM analysis of In(Zn)P cores (emission wavelength = 600 nm) and In(Zn)P@ZnSeS QDs (emission wavelength = 620 nm). The size of In(Zn)P QDs was estimated based on the assumption that the QDs were spherical and the diameter of at least 100 QDs in low magnification TEM images were measured. The size distribution of In(Zn)P QDs synthesized using the Zn oxo cluster was more uniform compared with that obtained from ZnOL. Moreover, for ZnOL as the precursor, we observed irregularly shaped ZnSeS shells and agglomerated In(Zn)P@ZnSeS QDs. This irregular shape induced a decrease in τ_{avg} and low PLQY after purification (Fig. S7 and Table S1†). After purification, the τ_{avg} of In(Zn)P@ZnSeS QDs prepared from ZnOL decreased to 26.45 ns, while that of In(Zn)P@ZnSeS QDs prepared from the Zn oxo cluster slightly increased to 40.6 ns. The PLQY of purified In(Zn)P QDs prepared from ZnOL was as low as 52%, and the contribution of fast decay increased from 0.18 to 0.26 upon shell growth (Table S1†). The low PLQY and the slow decay component may stem from the presence of exposed surface defects due to irregular shell shape and QD agglomeration. The combined results of TRPL, temperature-dependent PL, and TEM measurements suggested that the narrow FWHM of In(Zn)P QDs prepared from the Zn oxo cluster is due to the suppressed formation of surface defects and narrow size distribution. Thus, the adopted strategy (Zn oxo cluster + seed-mediated continuous growth) required one simple shelling step and afforded In(Zn)P@ZnSeS QDs with a narrow FWHM (~38 nm) and a high PLQY (>93%).

2.3. Ketonization reactions of Zn precursors during the synthesis of In(Zn)P QDs

Subsequently, we aimed to reveal why QDs prepared from Zn oxo cluster had a narrow FWHM than those prepared from the ZnOL. One of the challenges of using Zn precursors for the synthesis of In(Zn)P cores is the thermal decomposition of carboxylic acids at high temperature. Chaudret *et al.* confirmed the formation of hentriacotan-16-one through the ketonization (decarboxylative coupling) of indium palmitate using FT-IR spectroscopy.[36] After the injection of TMS_3P into the reaction mixture containing indium palmitate, the C═O band of hentriacotan-16-one started to be detectable. Importantly, water and CO_2 produced as ketonization byproducts could induce side reactions such as the surface oxidization of In(Zn)P cores and thus negatively affect optical properties.[37,38] Inspired by this approach, we also used FT-IR spectroscopy to probe the occurrence of ketonization (Fig. 3a). The C═O band of free Oleic acid (OA) at 1707 cm^{-1} disappeared when ZnOL and the Zn oxo cluster were formed which indicated fully bound of OA to Zn atoms. In the case of ZnOL, the asymmetric stretching of COO– (ν_aCOO^-), the scissoring vibration of δ_{CH2}, and the symmetric stretching of COO^- (ν_sCOO^-) were detected at 1525, 1464, and 1398 cm^{-1}, respectively.[39] In the case of the Zn oxo cluster, ν_aCOO^- and ν_sCOO^- were detected at higher wavenumbers of 1593 and 1423 cm^{-1}, respectively, which was ascribed to structural effects. Interestingly, for the Zn oxo cluster, we observed a peak at 1718 cm^{-1}, which was located at a slightly higher wavenumber than the C═O vibration of OA and was not observed for ZnOL. This peak was assigned to a ketonization product formed during the synthesis of the Zn oxo cluster at high temperature (320 °C, 2 h). Thus, the Zn oxo cluster did not undergo ketonization during the synthesis of In(Zn)P QDs, as it had already experienced ketonization. To validate the (non-) occurrence of ketonization during the synthesis of In(Zn)P QDs, we recorded the FT-IR spectra of non-purified aliquots of the reaction mixture (Fig. 4b and c and Fig. S8†). When ZnOL was used as the Zn precursor, the C═O peaks at 1713 and 1722 cm^{-1} started to be detected at 280 °C and after the injection of TMS_3P, which indicated the occurrence of ketonization during the synthesis of In(Zn)P QDs. However, in the case of the Zn oxo cluster, the Zn precursor already featured a C═O peak at 1718 cm^{-1}, and the intensity of this peak did not increase at any time during the reaction. Thus, we concluded that ketonization occurring when ZnOL was used as a Zn precursor produced byproducts such as water and CO_2, which could induce the surface oxidation of In(Zn)P cores and thus make their optical properties inferior to those of In(Zn)P cores produced from the Zn oxo cluster.

2.4. Effect of the Zn precursors on surface oxidation and other parameters affect size uniformity

The surface oxidation states of In(Zn)P cores were probed by XPS (Fig. 4d). Compared to those of In(Zn)P cores synthesized from ZnOL, the In $3d_{5/2}$ and In $3d_{3/2}$ peaks of In(Zn)P cores synthesized from the Zn oxo cluster were shifted to lower binding energies (by 0.4 and 0.6 eV, respectively), which reflects a difference in overall electronegativity due to surface oxidation by *in situ* generated byproducts. Subsequently, we prepared In(Zn)P cores in the presence of a small amount of deliberately introduced water (Fig. 4e). As we expected, the addition of water increased the FWHM of In(Zn)P cores, which was ascribed to the negative impact of surface oxidation by water molecules. In another control experiment, excess OA was added during the growth of In(Zn)P cores to probe the effects of carboxylate-induced side reactions (Fig. S9†), and FWHM increased with increasing OA content. Considering the ketonization reaction of ZnOL and the surface oxidation induced by water or carboxylic acid, the superior optical properties of In(Zn)P cores synthesized using the Zn oxo cluster were attributed to the suppression of ketonization and, hence, to the reduced *in situ* generation of byproducts.

In addition to exploiting the effect of the Zn oxo cluster, we probed the effects of a mild reducing agent, as the suppression of surface oxidation is crucial for the formation of monodisperse In(Zn)P QDs. Numerous works suggested the importance of suppressing InP core oxidation for growing red-emitting InP QDs. For example, Jang *et al.* used HF treatment before shell coating for the reduction of InP cores,[32] while Peng *et al.* coated a thin shell of ZnSe on InP cores to prevent

Published on 04 February 2022. Downloaded by Yunnan University on 8/23/2025 9:48:06 PM.

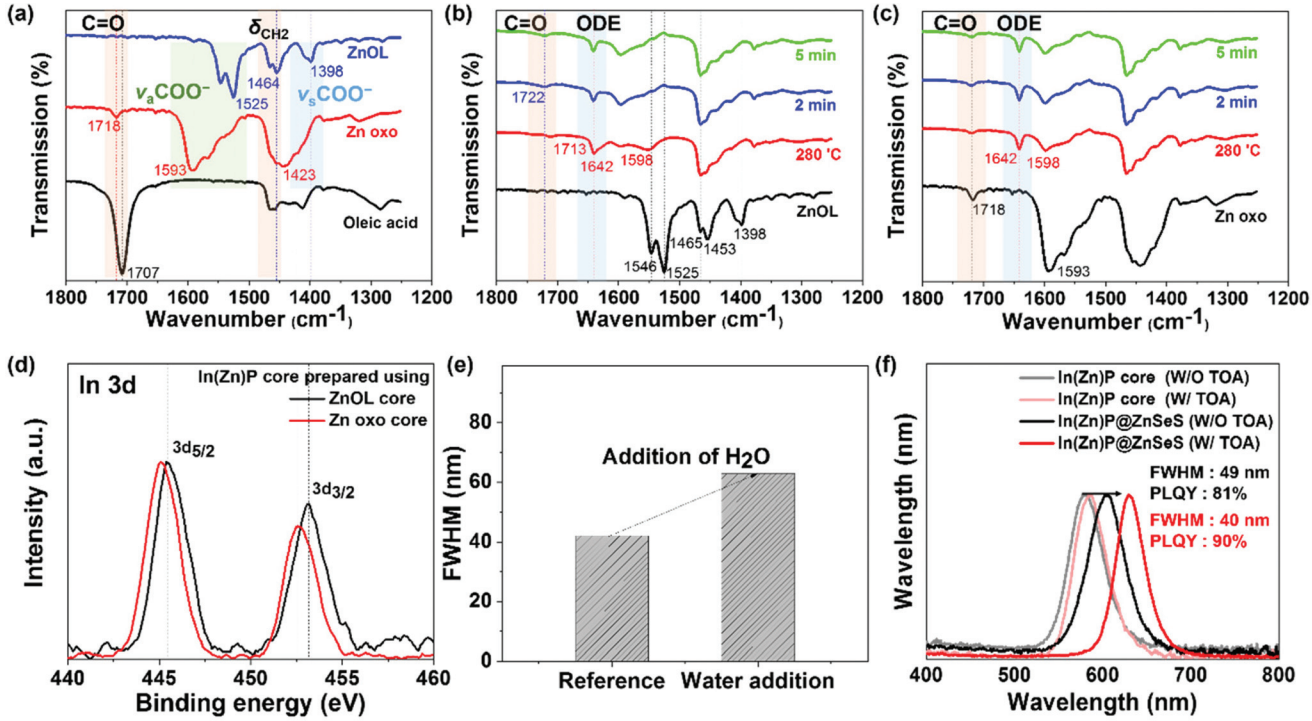

Fig. 4 (a) FT-IR spectra of OA and Zn precursors. FT-IR spectra of aliquots of In(Zn)P core solutions for (b) ZnOL and (c) Zn oxo cluster as precursors. (d) In 3d X-ray photoelectron spectra of In(Zn)P cores prepared from different Zn precursors. (e) Effect of water addition on the FWHM of In(Zn)P cores. (f) Effect of mild reducing agent on the optical properties of In(Zn)P QDs.

their oxidation during subsequent purification.[33] In our approach, the suppression of surface oxidation is also important for securing the high quality of In(Zn)P QDs. Therefore, we tested several reducing agents and optimized the reaction parameters to yield a narrow FWHM and a high PLQY (Fig. 4f and Fig. S10†). The reducing agent was introduced into the In(Zn)P seed solution, and the (Zn)In–P complex was injected to grow the In(Zn)P cores. Trioctylamine(TOA) and hexadecanediol were selected as mild reducing agents, while diisobutylaluminum hydride solution and the alane *N*,*N*-dimethylethylamine complex were selected as strong reducing agents. When TOA was used, the FWHM of In(Zn)P cores decreased from 49 to 40 nm, while the PLQY of In(Zn)P@ZnSeS QDs increased from 81 to 90% (compared to the case when no reducing agent was injected), which means that the injection of mild reducing agents could create a reducing environment around the surface of In(Zn)P cores and suppress their surface oxidation during growth. And there are optimal amount of TOA for high quality of In(Zn)P QDs because the excess of TOA may increase the reactivity of (Zn)In–P complex which resulted in the increase of FWHM (Fig. S10b†). XPS measurements revealed that the surface of In(Zn)P cores prepared with TOA was less oxidized than that of the cores prepared without TOA (Fig. S10a†). Moreover, we could observe the significant redshift of emission peak of In(Zn)P@ZnSeS QDs with TOA as reducing agent which might be the evidence of less oxidized surface and effective growth of ZnSeS shell. When strong reducing agents were used, In metal and bulk InP were obtained, and green-emitting In(Zn)P cores with low PLQYs and large FWHMs were synthesized because of (Zn)In–P complex nucleation (Fig. S10†). In addition to reducing agent presence/type, the In : P precursor ratio at the time of In(Zn)P seed formation is another important factor to consider when aiming for low FWHMs and high PLQYs. As the injection rate of the (Zn)In–P complex was constant, the uniform growth of In(Zn)P cores depended on the concentration of In(Zn)P seeds, which, in turn, was greatly affected by the In : P precursor ratio. For example, at an In : P ratio of 1 : 0.5, the FWHM of In(Zn)P cores during growth was maintained, whereas an increase in FWHM was observed for higher contents of the P precursor (Fig. S11†).

2.5. Fabrication and characterization of red-emitting QLEDs

Finally, we used In(Zn)P@ZnSeS core@shell QDs to fabricate QLEDs with PEDOT:PSS and PTAA as the hole injection layer and ZnO nanoparticles as the electron injection layer. The band energy diagram of the optimized device structure is presented in Fig. 5a. The corresponding electroluminescence (EL) peak was located at 631 nm and had a narrow FWHM of 47 nm (Fig. 5b). This emission corresponded to Commission Internationale de l'Eclairage (CIE) color coordinates of (0.69, 0.31), which fully covers the standard colors of the National Television System Committee (NTSC) (Fig. S12†). The optimized QLEDs exhibited a maximum luminescence of 1164 cd

 This journal is © The Royal Society of Chemistry 2022

Published on 04 February 2022. Downloaded by Yunnan University on 8/23/2025 9:48:06 PM.

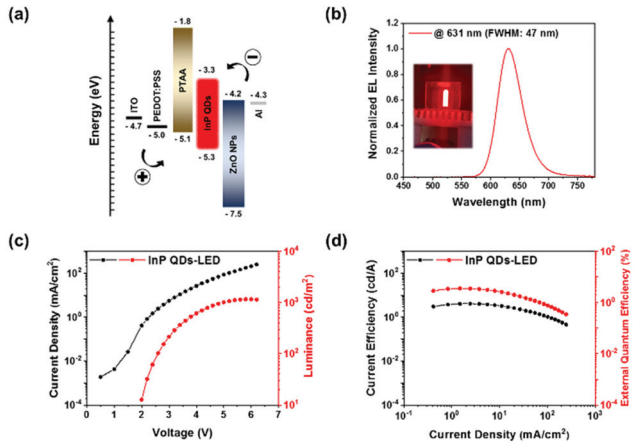

Fig. 5 Characteristics of optimized QLEDs based on red-emitting In(Zn)P QDs. (a) Band energy diagram, (b) EL spectrum, (c) current density and luminance as functions of voltage, and (d) current efficiency and external quantum efficiency as functions of current density.

m^{-2} and an external quantum efficiency of 3.61% (Fig. 5c and d). Detail device characteristics are summarized in Table S2.† In addition to the optimized device performance, we collected the performance of 15 QLED devices with the average EQEs was 3.39 ± 0.14% (Fig. S13†) to prove the reproducibility of our QLED devices. Moreover, the stability of QLED EL spectra was measured during device operation as the bias voltage increased from 2 to 6 V (Fig. S14†). As a result, the position and FWHM of the EL peak remained unchanged, which indicated superior spectral stability. Thus, the red-emitting In(Zn)P@ZnSeS QDs synthesized using the Zn oxo cluster were successfully used to construct QLEDs.

3. Conclusion

A strategy combining the use of a Zn oxo cluster as a Zn precursor and seed-mediated continuous growth was used to obtain red-emitting In(Zn)P QDs with a high PLQY (>93%) and a narrow FWHM (~38 nm). The adopted approach hindered the fast depletion of the P precursor, prevented secondary nucleation during the growth step, and suppressed the *in situ* generation of byproducts such as water. Mild reducing agents were concluded to minimize surface oxidation during core growth and promote the formation of size-uniform In(Zn)P cores. The prepared In(Zn)P@ZnSeS QDs were used to fabricate QLEDs that exhibited a maximum brightness of 1164 cd m^{-2} and an external quantum efficiency of 3.61%.

4. Experimental section

4.1 Materials

$Zn(CH_3COO)_2$ (99.99%), $In(acac)_3$ (acac = acetylacetonate; ≥99.99% trace metal basis), $Zn(acac)_2$ (for synthesis), $InCl_3$ (anhydrous; 99.999% trace metal basis), Se (99.99% trace metal basis), S (99.5%), 1-octadecene (ODE; 90%), oleic acid (OA; 90%), trioctylphosphine (TOP; 90%), trioctylamine (TOA; 98%), *n*-hexane (anhydrous; 95%), and acetone (99.5%) were obtained from Sigma-Aldrich. TMS_3P (99.0%) was obtained from SK Chemicals.

4.2 Preparation of precursors

4.2.1 TOP-Se (1 M). Se powder (0.789 g, 10 mmol) was dissolved in TOP (10 mL) at 70 °C in an Ar-filled glovebox.

4.2.2 TOP-S (1 M). S powder (0.32 g, 10 mmol) was dissolved in TOP (10 mL) at 70 °C in an Ar-filled glovebox.

4.2.3 $InCl_3$-TOP (0.5 M). $InCl_3$ powder (0.221 g, 1 mmol) was dissolved in TOP (2 mL) at 70 °C in an Ar-filled glovebox.

4.2.4 TMS_3P-TOP. TMS_3P (0.2 mL) was dissolved in TOP (2.5 mL) at 25 °C in an Ar-filled glovebox.

4.3 Synthesis of Zn oxo cluster

$Zn(CH_3COO)_2$ (2.75 g, 15 mmol) was mixed with OA (9.5 mL, 30 mmol) in a three-neck flask, and the mixture was dried under vacuum for 1 h at 25 °C and heated to 180 °C over 20 min, maintained at this temperature for 1 h under vacuum, purged with Ar, heated to 320 °C over 20 min, and maintained at this temperature for 2.5 h. The resulting solution containing the Zn oxo cluster ($[Zn_4O(oleate)_6]$ and $[Zn_7O_2(oleate)_{10}]$) was transferred to an Ar-filled glovebox without purification and used for further experiments.

4.4 Synthesis of (Zn)In–P complex

The (Zn)In–P complex was synthesized by the method of Ramasamy *et al.* with minor modifications.[31] $In(acac)_3$ (0.4121 g, 1 mmol), $Zn(acac)_2$ (0.1318 g, 0.5 mmol), OA (1.27 mL, 4 mmol), and ODE (10 mL) were mixed in three-neck flask, and the mixture was degassed at 120 °C for 1 h at 15 mTorr and cooled to 25 °C under Ar. After cooling, TMS_3P (0.19 mL TMS_3P in 1 mL TOP) solution was injected, and the mixture was stirred vigorously for 1 h. The resulting (Zn)In–P complex was used without further purification.

4.5. Synthesis of In(Zn)P cores by seed-mediated continuous growth

The $InCl_3$-TOP solution (0.2 mL) and the Zn oxo cluster (2 mmol) were mixed with ODE (8 mL) in a three-neck flask, and the mixture was degassed at 120 °C for 1 h, purged with Ar, and heated to 280 °C to induce In(Zn)P nucleation. At 280 °C, the TMS_3P-TOP solution (0.27 mL) was injected, and the mixture was allowed to react for 10 min. Subsequently, TOA (0.88 mL) was rapidly injected, and the (Zn)In–P complex was then injected at 1 mL h^{-1} using a syringe pump to obtain In(Zn)P cores of the desired size. The cores were precipitated by the addition of excess acetone and re-dispersed in hexane, and these purification steps were repeated two more times.

4.6. Synthesis of In(Zn)P@ZnSeS QDs

Instead of purification, the mixture containing In(Zn)P cores was cooled to 150 °C under Ar flow, supplemented with TOP-Se (0.6 mL, 1 M) and TOP-S (0.3 mL, 1 M), heated to

Published on 04 February 2022. Downloaded by Yunnan University on 8/23/2025 9:48:06 PM.

320 °C over 20 min, and held at this temperature for 1 h to produce a ZnSeS shell. The mixture was then cooled to 25 °C and purified as described above for In(Zn)P cores.

4.7. Device fabrication

Indium tin oxide (ITO) substrates were immersed in deionized water and cleaned under ultrasonication (200 W) for 15 min. Sequentially, acetone, then isopropyl alcohol were used to clean the ITO substrate. Finally, ITO substrates were dried in an oven (120 °C) for 1 h and treated with ozone for surface hydrophilization, spin-coated with poly(3,4-ethylenedioxythiophene):polystyrene sulfonic acid (PEDOT:PSS) solution at 3000 rpm for 40 s, and annealed at 150 °C for 15 min. After cooling, the substrates were transferred into a glovebox filled with N_2, spin-coated with poly(triaryl amine) (PTAA; 8 mg mL^{-1} in chlorobenzene) at 4000 rpm for 60 s, annealed at 140 °C for 20 min, cooled, and sequentially spin-coated with InP QDs (6 mg mL^{-1} in hexane) at 4000 rpm for 60 s and ZnO nanoparticles (20 mg mL^{-1} in methanol) at 3000 rpm for 30 s. Finally, Al (100 nm) was thermally deposited as an electrode under high vacuum (<10^{-6} Torr). The device active area equaled 13.5 mm^2.

4.8. Characterization

Absorption spectra were recorded on a UV-1800 (Shimadzu, Japan). Photoluminescence (PL) spectra were recorded on an Cary eclipse fluorescence spectrometer (Agilent, USA). Fourier transform infrared (FT-IR) spectra were recorded on a IRTracer-100 (Shimadzu, Japan). Time-resolved PL (TRPL) measurements were performed in a time-correlated single-photon-counting setup (Fluo-Time 300, PicoQuant, Germany) at 25 °C. Quantum efficiency was measured on an QE-2000 (Otsuka, Japan). Transmission electron microscopy (TEM) imaging (JEOL JEM-2100, Japan) was per-formed at an acceleration voltage of 200 kV using Cu grids (Ted Pella, USA). Samples for TEM imaging were prepared by placing a drop of a diluted QD solution in hexane on the grid and allowing it to dry. X-ray photoelectron spectroscopy (XPS) measurements were carried out using a K-Alpha spectrometer (ThermoFisher, USA). Samples for XPS analysis were prepared by placing a drop of the QD solution in hexane on a B-doped Si wafer followed by solvent evaporation. X-ray diffraction (XRD) was carried out with a D/MAX2500 V/PC (Rigaku, Japan) operated at 40 kV/200 mA using Cu Kα line (λ = 1.5405 Å). Dynamic light scattering (DLS) measurement were performed on a Zetasizer Nano-ZS90 (Malvern, UK) at 25 °C.

Author contributions

Conceptualization: Y. Choi, D. Kim, J. Park. Methodology: Y. Choi. Formal analysis: Y. Choi. Investigation: Y. Choi, D. Kim, Y. S. Shin. Writing-original draft: Y. Choi, D. Kim, Y. S. Shin. Validation: Y. S. Shin. Project administration: S. Orr, J. Y. Kim, J. Park. Funding acquisition: S. Orr, J. Park. Writing-review & editing: J. Y. Kim, J. Park. Supervision: J. Y. Kim, J. park.

Conflicts of interest

There are no conflicts to declare.

Acknowledgements

This work was supported by the National Research Foundation (NRF) grants funded by the Korean government (No. NRF-2017M3A7B6052456, NRF-2019R1A2C1010435, NRF-2021M3H4A3A01062963), the 2021 Research Fund (1.210047.01) of UNIST (Ulsan National Institute of Science & Technology), the Korea Medical Device Development Fund grant funded by the Korea Government (the Ministry of Science and ICT, the Ministry of Trade, Industry and Energy, the Ministry of Health & Welfare, the Ministry of Food and Drug Safety) (Project Number: 1711139070, KMDF_PR_20210525_0001), the Institute of Information & Communications Technology Planning & Evaluation (IITP) grant funded by the Korea Government (MSIT) (No. NRF-2021M3H4A3A01062963).

Notes and references

1 V. L. Colvin, M. C. Schlamp and A. P. Alivisatos, *Nature*, 1994, **370**, 354–357.
2 S. Coe, W. K. Woo, M. G. Bawendi and V. Bulovic, *Nature*, 2002, **420**, 800–803.
3 L. Qian, Y. Zheng, J. Xue and P. H. Holloway, *Nat. Photonics*, 2011, **5**, 543–548.
4 J. Kwak, W. K. Bae, D. Lee, I. Park, J. Lim, M. Park, H. Cho, H. Woo, D. Y. Yoon, K. Char, S. Lee and C. Lee, *Nano Lett.*, 2012, **12**, 2362–2366.
5 B. S. Mashford, M. Stevenson, Z. Popovic, C. Hamilton, Z. Zhou, C. Breen, J. Steckel, V. Bulovic, M. G. Bawendi, S. Coe-Sullivan and P. T. Kazlas, *Nat. Photonics*, 2013, **7**, 407–412.
6 H. Zhang, S. Chen and X. W. Sun, *ACS Nano*, 2018, **12**, 697–704.
7 K. Ding, Y. Fang, S. Dong, H. Chen, B. Luo, K. Jiang, H. Gu, L. Fan, S. Liu, B. Hu and L. Wang, *Adv. Opt. Mater.*, 2018, **6**, 1800347.
8 J. Song, O. Wang, H. Shen, Q. Lin, Z. Li, L. Wang, X. Zhang and L. S. Li, *Adv. Funct. Mater.*, 2019, **29**, 1808377.
9 J. Shen, Y. Zhu, X. Yang and C. Li, *Chem. Commun.*, 2012, **48**, 3686–3699.
10 P. Zrazhevskiy, M. Sena and X. Gao, *Chem. Soc. Rev.*, 2010, **39**, 4326–4354.
11 P. V. Kamat, *J. Phys. Chem. C*, 2008, **112**, 18737–18753.
12 A. J. Nozik, *Phys. E*, 2002, **14**, 115–120.
13 D. A. Hanifi, N. D. Bronstein, B. A. Koscher, Z. Nett, J. K. Swabeck, K. Takano, A. M. Schwartzberg, L. Maserati,

 This journal is © The Royal Society of Chemistry 2022

Published on 04 February 2022. Downloaded by Yunnan University on 8/23/2025 9:48:06 PM.

K. Vandewal, Y. van de Burgt, A. Salleo and A. P. Alivisatos, *Science*, 2018, **363**, 1199–1202.
14 A. Dutta, R. K. Behera, P. Pal, S. Baitalik and N. Pradhan, *Angew. Chem., Int. Ed.*, 2019, **58**, 5552–5556.
15 RoHS Compliance Guide, http://www.rohsguide.com/, 2021 (accessed 18 September, 2021).
16 G. Lin, Q. Ouyang, R. Hu, Z. Ding, J. Tian, F. Yin, G. Xu, Q. Chen, X. Wang and K. T. Yong, *Nanomedicine*, 2015, **11**, 341–350.
17 J. Cui, A. P. Beyler, L. F. Marshall, O. Chen, D. K. Harris, D. D. Wanger, X. Brokmann and M. G. Bawendi, *Nat. Chem.*, 2013, **5**, 602–606.
18 J. Park, J. Joo, S. G. Kwon, Y. Jang and T. Hyeon, *Angew. Chem., Int. Ed.*, 2007, **46**, 4630–4660.
19 P. M. Allen, B. J. Walker and M. G. Bawendi, *Angew. Chem., Int. Ed.*, 2010, **49**, 760–762.
20 D. Franke, D. K. Harris, L. Xie, K. F. Jensen and M. G. Bawendi, *Angew. Chem., Int. Ed.*, 2015, **54**, 14299–14303.
21 D. C. Gary, B. A. Glassy and B. M. Cossairt, *Chem. Mater.*, 2014, **26**, 1734–1744.
22 H. B. Chandrasiri, E. B. Kim and P. T. Snee, *Inorg. Chem.*, 2020, **59**, 15928–15935.
23 M. D. Tessier, D. Dupont, K. De Nolf, J. De Roo and Z. Hens, *Chem. Mater.*, 2015, **27**, 4893–4898.
24 J. H. Jo, D. Y. Jo, S. H. Lee, S. Y. Yoon, H. B. Lim, B. J. Lee, Y. R. Do and H. Yang, *ACS Appl. Nano Mater.*, 2020, **3**, 1972–1980.
25 E. Bang, Y. Choi, J. Cho, Y. H. Suh, H. W. Ban, J. S. Son and J. Park, *Chem. Mater.*, 2017, **29**, 4236–4243.
26 K. Kim, Y. H. Suh, D. Kim, Y. Choi, E. Bang, B. H. Kim and J. Park, *Chem. Mater.*, 2020, **32**, 2795–2802.
27 F. Pietra, L. De Trizio, A. W. Hoekstra, N. Renaud, M. Prato, F. C. Grozema, P. J. Baesjou, R. Koole, L. Manna and A. J. Houtepen, *ACS Nano*, 2016, **10**, 4754–4762.
28 N. Kirkwood, A. D. Backer, T. Altantzis, N. Winckelmans, A. Longo, F. V. Antolinez, F. T. Rabouw, L. D. Trizio, J. J. Geuchies, J. T. Mulder, N. Renau, S. Bals, L. Manna and A. J. Houtepen, *Chem. Mater.*, 2019, **32**, 557–565.
29 R. Toufanian, A. Piryatinski, A. H. Mahler, R. Iyer, J. A. Hollingsworth and A. M. Dennis, *Front. Chem.*, 2018, **6**, 567.
30 S. Tamang, C. Lincheneau, Y. Hermans, S. Jeong and P. Reiss, *Chem. Mater.*, 2016, **28**, 2491–2506.
31 P. Ramasamy, K. J. Ko, J. W. Kang and J. S. Lee, *Chem. Mater.*, 2018, **30**, 3643–3647.
32 Y. H. Won, O. Cho, T. Kim, D. Y. Chung, T. Kim, H. Chung, H. Jang, J. Lee, D. Kim and E. Jang, *Nature*, 2019, **575**, 634–638.
33 Y. Li, X. Hou, X. Dai, Z. Yao, L. Lv, Y. Jin and X. Peng, *J. Am. Chem. Soc.*, 2019, **141**, 6448–6452.
34 D. Franke, D. K. Harris, O. Chen, O. T. Bruns, J. A. Carr, M. W. B. Wilson and M. G. Bawendi, *Nat. Commun.*, 2016, **7**, 12749.
35 Y. Kim, S. Ham, H. Jang, J. H. Min, H. Chung, J. Lee, D. Kim and E. Jang, *ACS Appl. Nano Mater.*, 2019, **2**, 1496–1504.
36 A. Cros-Gagneux, F. Delpech, C. Nayral, A. Cornejo, Y. Coppel and B. Chaudret, *J. Am. Chem. Soc.*, 2010, **132**, 18147–18157.
37 M. D. Tessier, E. A. Baquero, D. Dupont, V. Grigel, E. Bladt, S. Bals, Y. Coppel, Z. Hens, C. Nayral and F. Delpech, *Chem. Mater.*, 2018, **30**, 6877–6883.
38 A. Vikram, A. Zahid, S. S. Bhargava, H. Jang, A. Sutrisno, A. Khare, P. Trefonas, M. Shim and P. J. A. Kenis, *ACS Appl. Nano Mater.*, 2020, **3**, 12325–12333.
39 J. J. Hermans, K. Keune, A. V. Loon and P. D. Iedema, *J. Anal. At. Spectrom.*, 2015, **30**, 1600–1608.